

Position Error Bound for Cooperative Sensing in MIMO-OFDM Networks

Lorenzo Pucci and Andrea Giorgetti

Abstract—This paper investigates the fundamental limits of target position estimation accuracy of joint sensing and communication (JSC) networks comprising several monostatic base stations (BSs) that cooperate to localize targets. Specifically, each BS adopts a multiple-input multiple-output (MIMO)-orthogonal frequency division multiplexing (OFDM) scheme with a multi-beam radiation pattern to partition power between communication and sensing tasks. Building on prior works, we derive a general framework to evaluate the positioning accuracy of a target in networks with an arbitrary number of cooperating BSs and arbitrary geometrical configurations using Fisher information. Numerical results demonstrate the benefits of cooperation between BSs in improving target localization accuracy and provide insights into the relationships between various system parameters, which may aid in designing JSC networks.

Index Terms—Fisher information, Cramér–Rao lower bound, joint sensing and communication, cooperative sensing, OFDM.

I. INTRODUCTION

Joint sensing and communication (JSC), namely the ability of mobile communication systems to jointly communicate and sense the environment, has emerged as a new paradigm for the upcoming 6G mobile networks. Research has recently demonstrated the effectiveness of orthogonal frequency division multiplexing (OFDM)-based communication systems in performing sensing tasks. In particular, several works have investigated the sensing performance of OFDM-based JSC systems in terms of root mean square error (RMSE) of target parameters estimation, mainly with monostatic and bistatic configurations [1]–[3]. Moreover, several works have investigated the performance of JSC systems in terms of Cramér–Rao lower bound (CRLB), mainly considering monostatic radar settings. In [4] and [5] narrowband monostatic JSC systems are considered. The CRLB is used as a performance metric of target estimation to study the trade-off between communication and sensing. In [6], the CRLB of position estimation is derived considering a monostatic JSC system in a vehicular scenario. However, to the best of the authors’ knowledge, there remains a gap in research regarding the investigation of fundamental limits of target position estimation accuracy by considering JSC networks in which multiple monostatic sensors cooperate to improve estimation accuracy.

Aiming to fill this gap, this work investigates the fundamental limits of target position estimation accuracy in a

This work was supported by the European Union under the Italian National Recovery and Resilience Plan (NRRP) of NextGenerationEU, partnership on “Telecommunications of the Future” (PE00000001 - program “RESTART”). The authors are with the Wireless Communications Laboratory, CNIT, DEI, University of Bologna, Italy, Email: {lorenzo.pucci3, andrea.giorgetti}@unibo.it

OFDM-based JSC network comprising monostatic multiple-input multiple-output (MIMO) base stations (BSs). These BSs cooperate to localize targets within the monitored area, using a multi-beam radiation pattern to share the transmit power between communication and sensing functions. Inspired from previous works [7]–[9], we derive a framework to calculate the position error bound (PEB) of target localization accuracy via Fisher information. In particular, we start deriving a closed-form solution to assess the CRLB of target position accuracy when only one BS is involved, using the concept of equivalent Fisher information matrix (EFIM). Then, we develop a general formulation for the PEB with multiple cooperative BSs by exploiting the additivity of Fisher information. Based on the theoretical framework, we examine the sensing coverage of the JSC network and analyze factors affecting localization accuracy, including the number of BSs, available bandwidth, number of antennas, and power allocation.

In this paper, we use capital boldface letters for matrices and lowercase bold letters for vectors. Additionally, $(\cdot)^T$ and $(\cdot)^H$ denote transpose and conjugate transpose, respectively; $\|\cdot\|$ is the Euclidean norm of vectors; $[\mathbf{X}]_{a:b,c:d}$ denotes a submatrix of \mathbf{X} composed of rows a to b and columns c to d ; \mathbf{I}_n is the $n \times n$ identity matrix, while $\text{Tr}(\cdot)$ is the trace of a square matrix. $\mathbb{E}\{\cdot\}$ and $\mathbb{V}(\cdot)$ represent mean value and variance, respectively. A zero-mean circularly symmetric complex Gaussian random vector with covariance Σ is denoted by $\mathbf{x} \sim \mathcal{CN}(\mathbf{0}, \Sigma)$. $|\cdot|$ is the absolute value operator.

The paper is organized as follows. Section II and Section III present the system model and the PEB derivation, respectively. Numerical results are given in Section IV, while Section V concludes the paper with some remarks.

II. SYSTEM MODEL FOR MONOSTATIC JSC

In this analysis, a network of monostatic OFDM-based JSC systems with multiple antennas is considered. Each BS consists of a transmitter (Tx) antenna array with N_T elements and of an receiver (Rx) antenna array with N_R elements. The system transmits a waveform with M OFDM symbols and K active subcarriers. The equivalent low-pass (ELP) representation of the signal transmitted by the n th antenna can be written as

$$s_n(t) = \sum_{m=0}^{M-1} \left(\sum_{k=0}^{K-1} x_n[k, m] e^{j2\pi \frac{k}{T} t} \right) g(t - mT_s) \quad (1)$$

where $x_n[k, m]$ is the complex modulation symbol to be transmitted on the k th subcarrier at time instant m , mapped through digital precoding at the n th transmitting antenna. Moreover,

$g(t)$ is the employed pulse, $\Delta f = 1/T$ is the subcarrier spacing, and $T_s = T + T_{CP}$ is the OFDM symbol duration including the cyclic prefix (CP). Without loss of generality, the constellation is normalized so that $\mathbb{E}\{|x_n[k, m]|^2\} = 1$.

A. Dual-functional waveform

We consider the case where the same symbol $x_n[k, m]$ is transmitted to all antennas via beamforming, i.e., $x_n[k, m] = x[k, m]$. Therefore, the vector collecting the signal samples at the antennas is $\mathbf{x}[k, m] = \mathbf{w}_T x[k, m] \in \mathbb{C}^{N_T \times 1}$, where $\mathbf{w}_T \in \mathbb{C}^{N_T \times 1}$ is the precoding vector, or beamformer (BF).

In this work, the vector \mathbf{w}_T is designed to have a multibeam radiation pattern so that the total transmit power of the OFDM signal is split between communication and sensing beams [10], [11]. Thus, the transmitting BF \mathbf{w}_T can be written as

$$\mathbf{w}_T = \sqrt{\rho} \mathbf{w}_{T,s} + \sqrt{1-\rho} \mathbf{w}_{T,c} \quad (2)$$

where $\rho \in [0, 1]$ is the parameter used to control the fraction of the total power apportioned to the two directions, while $\mathbf{w}_{T,c}$ and $\mathbf{w}_{T,s}$ are the communication and the sensing BFs, respectively. Without loss of generality, we employ beam-steering for both sensing and communication tasks. The literature also presents other beamforming methods, such as those based on optimization techniques, which can enhance performance further [12]. Accordingly, the BFs are defined as [13]

$$\mathbf{w}_{T,c} = \frac{\sqrt{P_{\text{avg}} G_T^a}}{N_T} \mathbf{a}(\theta_{T,c}), \quad \mathbf{w}_{T,s} = \frac{\sqrt{P_{\text{avg}} G_T^a}}{N_T} \mathbf{a}(\theta_{T,s}) \quad (3)$$

where G_T^a is the transmit array gain along the beam steering direction (where such a gain is maximum), $P_{\text{avg}} G_T^a$ is the average effective isotropic radiated power (EIRP) per subcarrier, being $P_{\text{avg}} = P_T/K$ with P_T the total transmit power. Moreover, $\mathbf{a}(\theta_{T,c}) \in \mathbb{C}^{N_T \times 1}$ and $\mathbf{a}(\theta_{T,s}) \in \mathbb{C}^{N_T \times 1}$ are the steering vectors related to communication and sensing, respectively. Considering uniform linear array (ULA) with N_a elements half-wavelength spaced and taking its center as a reference, the spatial steering vector at a given direction of arrival (DoA)/direction of departure (DoD) θ is [14, Chapter 9]

$$\mathbf{a}(\theta) = [e^{-i \frac{N_a-1}{2} \pi \sin \theta}, \dots, e^{i \frac{N_a-1}{2} \pi \sin \theta}]^T. \quad (4)$$

B. Received signal

The vector $\mathbf{r}[k, m] \in \mathbb{C}^{N_R \times 1}$ of the received symbols after the fast Fourier transform (FFT) block in the OFDM receiver, is given by¹

$$\mathbf{r}[k, m] = \mathbf{H}[k, m] \mathbf{x}[k, m] + \boldsymbol{\nu}[k, m] \quad (5)$$

where $\mathbf{H}[k, m] \in \mathbb{C}^{N_R \times N_T}$ is the MIMO channel matrix for the k th subcarrier at time m and $\boldsymbol{\nu}[k, m] \sim \mathcal{CN}(\mathbf{0}, \sigma_N^2 \mathbf{I}_{N_R})$ is the additive white Gaussian noise (AWGN) at Rx antennas with $\sigma_N^2 = N_0 \Delta f$. Here $N_0 = k_B T_0 n_F$ is the one-sided noise power spectral density (PSD), being k_B the Boltzmann

¹This notation represents a 3D array where each vector contains samples along the antennas, with one vector corresponding to each (k, m) pair.

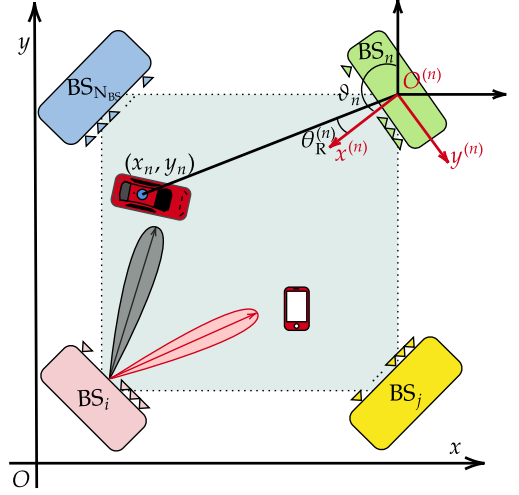


Fig. 1: An example of a cooperative JSC network of interest.

constant, T_0 the reference temperature and n_F the receiver noise figure.

Considering a tapped delay line channel model with reflections from L scatterers and line-of-sight (LoS) propagation conditions, the channel matrix can be written as

$$\mathbf{H}[k, m] = \sum_{l=1}^L \underbrace{\bar{\alpha}_l e^{i2\pi m T_s f_{D,l}} e^{-i2\pi k \Delta f \tau_l}}_{\triangleq \beta_l} \mathbf{b}(\theta_{R,l}) \mathbf{a}^H(\theta_{R,l}) \quad (6)$$

where τ_l , $f_{D,l}$, and $\theta_{R,l}$ are the round-trip delay, the Doppler shift, and the DoA of the l th target, respectively. The term $\bar{\alpha}_l = \alpha_l e^{j\phi_l}$ is the complex amplitude which includes phase shift and attenuation along the l th propagation path. According to the radar equation, $\alpha_l^2 = \frac{G_R c^2 \sigma_l}{(4\pi)^3 f_c^2 r_l^4}$, being c the speed of light, f_c the carrier frequency, r_l and σ_l the distance between the monostatic system and the scatterer l and the radar cross-section of the l th scatterer, respectively; G_R is the gain of the single Rx antenna element. Considering a single scatterer scenario, i.e., $L = 1$, and dropping the index l , the received signal in (5) simplifies into

$$\mathbf{r}[k, m] = \beta \mathbf{b}(\theta_R) \mathbf{a}^H(\theta_R) \mathbf{w}_T x[k, m] + \boldsymbol{\nu}[k, m]. \quad (7)$$

After removing the transmitted symbols, $x[k, m]$ (assumed to be known), which represent nuisance, through element-wise division, the received samples are obtained²

$$\mathbf{y}[k, m] = \beta \mathbf{h} + \mathbf{n}[k, m] \quad (8)$$

where $\mathbf{n}[k, m] \sim \mathcal{CN}(\mathbf{0}, \tilde{\sigma}_N^2[k, m] \mathbf{I}_{N_R})$ with $\tilde{\sigma}_N^2[k, m] = \sigma_N^2 / |x[k, m]|^2$, and $\mathbf{h} \triangleq \mathbf{b}(\theta_R) \mathbf{a}^H(\theta_R) \mathbf{w}_T$.³ Recalling that the noise after FFT blocks is white across the time, frequency, and spatial (antenna) domain, the log-likelihood function of the received ensemble $\mathcal{Y} = \{\mathbf{y}[k, m]\}_{k=0, \dots, K-1, m=0, \dots, M-1}$ is

²This approach is often called reciprocal filtering.

³Note that if a constant envelope modulation is used, e.g., quadrature phase shift keying (QPSK) then $\tilde{\sigma}_N^2[k, m] = \sigma_N^2$.

$$\mathcal{I}(\Theta) = \Gamma \times \begin{bmatrix} \frac{2}{\alpha^2} & 0 & 0 & 0 & 0 \\ 0 & 2 & 2\pi T_s(M-1) & -2\pi\Delta f(K-1) & 0 \\ 0 & 2\pi T_s(M-1) & \frac{4\pi^2 T_s^2(2M-1)(M-1)}{3} & -2\pi^2 T_s \Delta f(M-1)(K-1) & 0 \\ 0 & -2\pi\Delta f(K-1) & -2\pi^2 T_s \Delta f(M-1)(K-1) & \frac{4\pi^2 \Delta f^2(2K-1)(K-1)}{3} & 0 \\ 0 & 0 & 0 & 0 & \frac{\pi^2(N_R^2-1)\cos^2(\theta_R)}{6} \end{bmatrix} \quad (9)$$

$$\ln f(\mathcal{Y}) = - \sum_{k=0}^{K-1} \sum_{m=0}^{M-1} N_R \ln \tilde{\sigma}_N^2[k, m] + \frac{1}{\tilde{\sigma}_N^2[k, m]} \left\| \mathbf{y}[k, m] - \beta \mathbf{h} \right\|^2 \quad (10)$$

where we omitted those terms that are not relevant for the derivation of the Fisher information matrix (FIM).

III. POSITION ERROR BOUND WITH AND WITHOUT COOPERATION

A. Fisher information matrix and CRLB

The FIM of the vector of parameters $\Theta = (\alpha, \phi, f_D, \tau, \theta_R)^T$ is calculated from (10) as

$$[\mathcal{I}(\Theta)]_{i,j} = -\mathbb{E} \left\{ \frac{\partial^2 \ln f(\mathcal{Y})}{\partial \theta_i \partial \theta_j} \right\} \quad i, j = 1, \dots, 5 \quad (11)$$

$$= \sum_{k=0}^{K-1} \sum_{m=0}^{M-1} \mathbb{E} \left\{ \frac{|x[k, m]|^2}{\sigma_N^2} \frac{\partial^2}{\partial \theta_i \partial \theta_j} \left\| \mathbf{y}[k, m] - \beta \mathbf{h} \right\|^2 \right\}$$

By substituting (8) into (11) and following lengthy calculations, the FIM can be derived, as reported at the top of the next page in (9), where $\Gamma = \text{SNR} N_R K M$. Subsequently, inverting (9) yields the expression for the CRLB of each parameter:

$$\text{CRB}(\alpha) = [\mathcal{I}^{-1}]_{1,1} = \frac{\alpha^2}{2KM N_R \text{SNR}} \quad (12)$$

$$\text{CRB}(\phi) = [\mathcal{I}^{-1}]_{2,2} = \frac{7KM + K + M - 5}{2(K^2 + K)(M^2 + M) N_R \text{SNR}}$$

$$\text{CRB}(f_D) = [\mathcal{I}^{-1}]_{3,3} = \frac{3}{2\pi^2 T_s^2 K M (M^2 - 1) N_R \text{SNR}}$$

$$\text{CRB}(\tau) = [\mathcal{I}^{-1}]_{4,4} = \frac{3}{2\pi^2 \Delta f^2 M K (K^2 - 1) N_R \text{SNR}}$$

$$\text{CRB}(\theta_R) = [\mathcal{I}^{-1}]_{5,5} = \frac{6}{\pi^2 K M (N_R^2 - 1) N_R \text{SNR} \cos^2(\theta_R)}$$

By choosing \mathbf{w}_T according to (2), setting $\theta_{T,s} = \theta_R$ and considering sufficiently large N_T , the signal-to-noise ratio (SNR) at the single receiving antenna element is given by

$$\text{SNR} = \rho \frac{P_T G_T^a \alpha^2}{N_0 K \Delta f} = \rho \frac{P_T G_T^a G_R c^2 \sigma}{(4\pi)^3 f_c^2 r^4 N_0 K \Delta f} \quad (13)$$

B. PEB for a monostatic sensor

Let us define the target position as $\mathbf{p} = (x, y) = (r \cos(\theta_R), r \sin(\theta_R))$, the estimated position as $\hat{\mathbf{p}} = (\hat{x}, \hat{y}) = (\hat{r} \cos(\hat{\theta}_R), \hat{r} \sin(\hat{\theta}_R))$ and the error as $e_p = \|\hat{\mathbf{p}} - \mathbf{p}\| = \sqrt{(x - \hat{x})^2 + (y - \hat{y})^2}$. The CRLB for the target position

estimation in monostatic sensing can be calculated retaining only the information of the FIM (9) related to τ and θ_R via the EFIM [8]. Given the parameter vector $\Theta = (\alpha, \phi, f_D, \tau, \theta_R)^T$ we partition it into $\Theta = [\Theta_1^T, \Theta_2^T]^T$ with $\Theta_1 = (\alpha, \phi, f_D)^T$ $\Theta_2 = (\tau, \theta_R)^T$, which induces the partition of the FIM into the matrices $\mathbf{A} \in \mathbb{R}^{3 \times 3}$, $\mathbf{B} \in \mathbb{R}^{3 \times 2}$, and $\mathbf{C} \in \mathbb{R}^{2 \times 2}$, as $\mathcal{I}(\Theta) = \begin{bmatrix} \mathbf{A} & \mathbf{B} \\ \mathbf{B}^T & \mathbf{C} \end{bmatrix}$. Then, the EFIM is

$$\mathcal{I}_e(\Theta_2) = \mathbf{C} - \mathbf{B}^T \mathbf{A}^{-1} \mathbf{B} \quad (14)$$

$$= \text{SNR} N_R K M \times \begin{bmatrix} \frac{2\pi^2 \Delta f^2 (K^2 - 1)}{3} & 0 \\ 0 & \frac{\pi^2 (N_R^2 - 1) \cos^2(\theta_R)}{6} \end{bmatrix}$$

known as the Schur complement of \mathbf{A} .⁴ Since we are interested in the CRLB of position estimation, we need a reparameterization to calculate the EFIM in (14) for \mathbf{p} , i.e.,

$$\mathcal{I}_e(\mathbf{p}) = \mathbf{J}_m^T \mathcal{I}_e(\Theta_2) \mathbf{J}_m \quad (15)$$

where \mathbf{J}_m is the Jacobian of the transformation $\{\theta_R = \arctan(y/x), \tau = \frac{2}{c} \sqrt{x^2 + y^2}\}$, which corresponds to

$$\mathbf{J}_m = \begin{bmatrix} \frac{\partial \tau}{\partial x} & \frac{\partial \tau}{\partial y} \\ \frac{\partial \theta_R}{\partial x} & \frac{\partial \theta_R}{\partial y} \end{bmatrix} = \begin{bmatrix} \frac{2}{c} \frac{x}{\sqrt{x^2 + y^2}} & \frac{2}{c} \frac{y}{\sqrt{x^2 + y^2}} \\ -\frac{y}{x^2 + y^2} & \frac{x}{x^2 + y^2} \end{bmatrix} \quad (16)$$

Hence, the CRLB is

$$\mathbb{V}\{e_p\} \geq \text{CRB}(\mathbf{p}) = \text{Tr}(\mathcal{I}_e^{-1}(\mathbf{p})) \quad (17)$$

$$= \text{Tr}(\mathbf{J}_m^{-1} \mathcal{I}_e^{-1}(\Theta_2) [\mathbf{J}_m^{-1}]^T)$$

$$= \text{Tr}(\mathcal{I}_e^{-1}(\Theta_2) [\mathbf{J}_m^{-1}]^T \mathbf{J}_m^{-1}) = \text{Tr}(\mathcal{I}_e^{-1}(\Theta_2) \mathbf{M}_m)$$

where $\mathbf{M}_m = \text{diag}(c^2/4, x^2 + y^2)$. Therefore, we get

$$\text{CRB}(\mathbf{p}) = \frac{c^2}{4} [\mathcal{I}^{-1}]_{4,4} + r^2 [\mathcal{I}^{-1}]_{5,5} \quad (18)$$

$$= \frac{6}{\pi^2 K M N_R \text{SNR}} \left[\frac{c^2/16}{\Delta f^2 (K^2 - 1)} + \frac{r^2}{(N_R^2 - 1) \cos^2(\theta_R)} \right]$$

From (18) we have $\text{PEB} = \sqrt{\text{CRB}(\mathbf{p})}$.

C. PEB for a network of cooperative monostatic sensors

Let us consider a JSC network consisting of N_{BS} monostatic BSs that cooperate to monitor a given area, as shown in Fig. 1.⁵ Let $\mathbf{O}^{(n)} = (x_R^{(n)}, y_R^{(n)})$ and $\mathbf{p} = (x, y)$ be the position of the n th monostatic BS and of a generic point-like target, respectively, in a common Cartesian reference system. Moreover, let $\mathbf{p}^{(n)} = (x_n, y_n)$ and $\theta_R^{(n)}$ be the position and the

⁴One interesting property is that $[\mathcal{I}^{-1}(\Theta)]_{4:5,4:5} = \mathcal{I}_e^{-1}(\Theta_2)$, so the EFIM retains all the necessary to derive the information inequality for Θ_2 .

⁵We assume that BSs can operate using either time or frequency division among themselves to avoid interference.

DoA of the target, respectively, with respect to the n th local reference system centered at $\mathbf{O}^{(n)}$. The relation between \mathbf{p} and $\mathbf{p}^{(n)}$ is $\{x_n = x' \cos(\vartheta_n) + y' \sin(\vartheta_n), y_n = -x' \sin(\vartheta_n) + y' \cos(\vartheta_n)\}$, where $x' = x - x_R^{(n)}$ and $y' = y - y_R^{(n)}$, while ϑ_n is the counterclockwise rotation angle of the n th reference system with respect to the standard one.

Considering that each of the N_{BS} BSs performs target position estimation independently from the others, the FIM for cooperative position estimation is given by

$$\mathcal{I}_e(\mathbf{p}) = \sum_{n=1}^{N_{\text{BS}}} \mathbf{J}_n^T \mathcal{I}_e(\mathbf{p}^{(n)}) \mathbf{J}_n \quad (19)$$

where $\mathcal{I}_e(\mathbf{p}^{(n)})$ represents the EFIM for the target position $\mathbf{p}^{(n)}$ as seen by the n th BS. The elements of $\mathcal{I}_e(\mathbf{p}^{(n)})$ are computed according to (15) by setting $(x, y) = (x_n, y_n)$ and $\theta_R = \theta_R^{(n)}$, and given by

$$\mathcal{I}_e(\mathbf{p}^{(n)}) = \xi_n \begin{bmatrix} a x_n^2 r_n^2 + b y_n^2 & x_n y_n (a r_n^2 - b) \\ x_n y_n (a r_n^2 - b) & a y_n^2 r_n^2 + b x_n^2 \end{bmatrix} \quad (20)$$

where $a = 16\Delta f^2(K^2 - 1)$, $b = c^2(N_R^2 - 1)\cos^2(\theta_R^{(n)})$, r_n is the Euclidean distance between the target and the n th BS, and $\xi_n = \frac{\pi^2 K M N_R \text{SNR}_n}{6c^2 r_n^4}$. In ξ_n , SNR_n is the SNR computed according to (13) with respect to the n th BS. Note that, \mathbf{J}_n in (19) represents the Jacobian of the transformation $n : (x, y) \rightarrow (x_n, y_n)$, defined as

$$\mathbf{J}_n = \begin{bmatrix} \frac{\partial x_n}{\partial x} & \frac{\partial x_n}{\partial y} \\ \frac{\partial y_n}{\partial x} & \frac{\partial y_n}{\partial y} \end{bmatrix} = \begin{bmatrix} \cos(\vartheta_n) & \sin(\vartheta_n) \\ -\sin(\vartheta_n) & \cos(\vartheta_n) \end{bmatrix}. \quad (21)$$

After computing (19), the PEB for a system composed of N_{BS} BSs, which cooperate to perform target localization in a given area can be obtained as the square root of $\text{CRB}(\mathbf{p})$, computed according to the first line of (17).

IV. NUMERICAL RESULTS

In this section, we provide some numerical results to analyze the fundamental limits of target localization accuracy for a cooperative JSC network. The analytical framework introduced in Section III is used to evaluate the PEB in the presence of a variable number N_{BS} of BSs, up to 4, considering a single scatterer scenario and the system parameters in Table I. Without loss of generality, we consider the BSs to be positioned at the corners of a square area of side 100 m, with the Tx/Rx ULAs of each BS pointing toward the center of the square, as shown in Fig. 1. In particular, starting from the BS in the lower left corner of the square and moving counterclockwise, the following vector of rotation angles is considered $\vartheta = \{\pi/4, \pi - \pi/4, \pi + \pi/4, -\pi/4\}$.

Two types of analysis are conducted. The first involves varying the target position within the designated area while keeping all the system parameters constant. Conversely, the target position remains fixed in the second analysis while one parameter among K , ρ , and N_R , is varied.

TABLE I: JSC network parameters

Parameters [5G NR]	Symbols	Values
Number of Rx antennas	N_R	16
Carrier frequency	f_c	28 GHz
OFDM symbols (time slots)	M	112
Active subcarriers	K	744
Subcarrier spacing	Δf	120 kHz
Total EIRP	$P_T G_T^a$	30 dBm
Fraction of power for sensing	ρ	0.1
Power spectral density	N_0	$4 \cdot 10^{-20}$ W/Hz
Target radar cross-section	σ	1 m ²

A. PEB vs target position

This section analyzes target localization accuracy in the considered area using heatmaps. The target is moved within the area, and for each position, the PEB is computed as described in Section III-C. It is important to note that for an unbiased estimator, the PEB serves as a lower bound for the RMSE of target position estimation. Thus, this analysis provides valuable insights into the coverage capabilities of a JSC network with a specified number N_{BS} of monostatic BSs. For instance, by setting a predefined minimum PEB, one can perform a coverage analysis of the sensing functionality.

The results are presented in Fig. 2, where the PEB is computed for cooperative scenarios involving two, three, and four BSs. Notably, satisfactory localization accuracy can be achieved with just two BSs, attaining a maximum PEB of approximately 0.25 m. This is observed even in the worst-case scenario, where the target is equidistant from both BSs, as illustrated in Fig. 2a. Furthermore, the maximum PEB decreases by approximately 30% and 60% when three and four BSs cooperate, as shown in Fig. 2b and Fig. 2c, respectively.

B. PEB vs system parameters

In this analysis, the target position is fixed at the center of the square, specifically at coordinates (50, 50) m, and the PEB is computed while varying K , ρ , and N_R . The aim is to explore which parameters prominently influence localization accuracy. The results are shown in Fig. 3 where red dots indicate PEB values computed with all the parameters set according to Table I. Fig. 3a reveals that allocating many subcarriers for sensing may not be advantageous in cooperative networks with up to two BSs. Conversely, increasing the number of BSs significantly improves localization accuracy. In Fig. 3b, the impact of the number of antennas at the Rx, N_R , is shown by considering up to 264 antenna elements. Notably, increasing N_R greatly enhances localization performance, enabling sub-centimeter accuracy when $N_R \geq 180$ and $N_{\text{BS}} \geq 3$.

Lastly, Fig. 3c shows the impact of the fraction of power reserved for sensing. It is possible to observe that increasing ρ notably affects overall accuracy, although less than increasing N_R . However, selecting high ρ is discouraged due to its adverse effect on communication performance resulting from power allocation. As for the previous analysis, the benefit of cooperation is evident, as increasing N_{BS} leads to lower PEB.

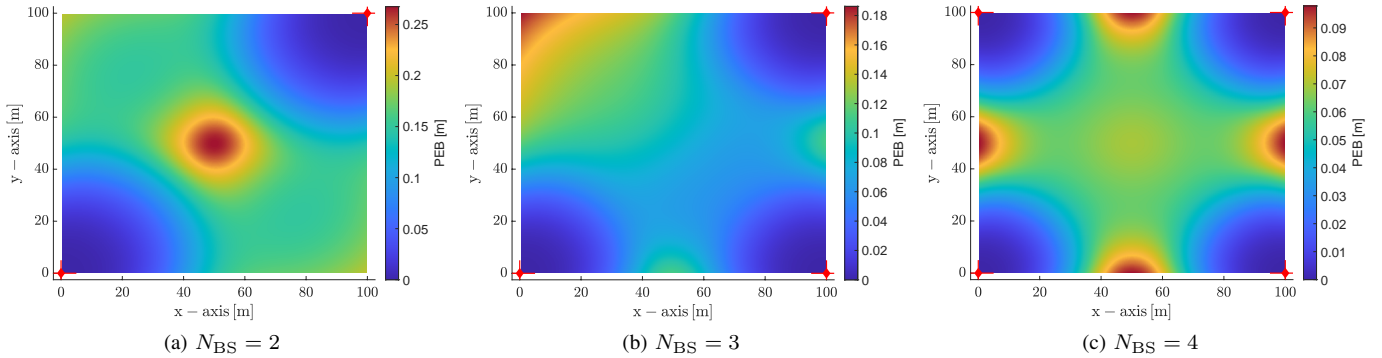


Fig. 2: Heatmaps showing the PEB of position estimation for a JSC network composed of $N_{\text{BS}} = \{2, 3, 4\}$ monostatic BSs, in a), b), and c), respectively. The heatmaps are computed inside the monitored area according to the system parameters in Table I. The active BSs are indicated by red markers.

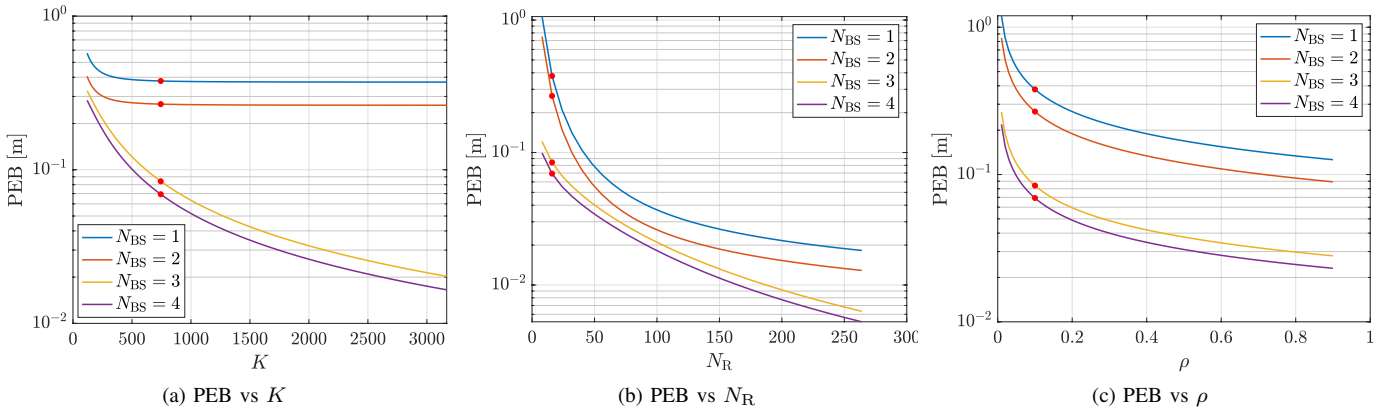


Fig. 3: PEB as a function of: a) the number of active subcarriers K , b) the number of antennas N_{R} at Rx, c) the fraction of power reserved for sensing ρ . Red dots correspond to the PEB calculated by fixing the values of K , ρ , and N_{R} as in Table I. Also, the number of BSs, N_{BS} , is varied.

V. CONCLUSION

In this work, we have derived and explored the fundamental limits of target localization accuracy within a cooperative JSC network comprising multiple monostatic MIMO-OFDM BSs. Utilizing the additivity property of Fisher information, we derived a framework to assess target positioning accuracy, using the PEB metric, for an arbitrary geometrical configuration. Our numerical analyses underscore the advantages of cooperative approaches, revealing that an increase in the number of BSs enhances localization performance and the sensing system’s coverage despite constraints on power, bandwidth, and antenna arrays. Notably, our results indicate that the number of receiving antennas is pivotal in boosting localization accuracy.

REFERENCES

- [1] M. Braun, “OFDM radar algorithms in mobile communication networks,” Ph.D. dissertation, Karlsruhe Institute of Technology, 2014.
- [2] D. Tagliaferri, M. Mizmizi, S. Mura, F. Linsalata, D. Scazzoli, D. Badini, M. Magarini, and U. Spagnolini, “Integrated sensing and communication system via dual-domain waveform superposition,” *IEEE Trans. Wireless Commun.*, 2023.
- [3] L. Pucci, E. Matricardi, E. Paolini, W. Xu, and A. Giorgetti, “Performance analysis of a bistatic joint sensing and communication system,” in *IEEE Int. Conf. Commun. (ICC) Workshops*, Seoul, Republic of Korea, May 2022, pp. 73–78.
- [4] F. Liu, Y.-F. Liu, A. Li, C. Masouros, and Y. C. Eldar, “Cramér-Rao bound optimization for joint radar-communication beamforming,” *IEEE Transactions on Signal Processing*, vol. 70, pp. 240–253, Dec. 2021.
- [5] F. Zabini, E. Paolini, W. Xu, and A. Giorgetti, “Joint sensing and communications in finite block-length regime,” in *IEEE Global Comm. Conf. (Globecom)*, 2022, pp. 5595–5600.
- [6] C. Giovannetti, N. Decarli, S. Bartoletti, R. A. Stirling-Gallacher, and B. M. Masini, “Target positioning accuracy of V2X sidelink joint communication and sensing,” *IEEE Wireless Commun. Lett.*, vol. 13, no. 3, pp. 849–853, Mar. 2024.
- [7] Y. Shen and M. Z. Win, “Fundamental limits of wideband localization—part I: A general framework,” *IEEE Trans. Inf. Theory*, vol. 56, no. 10, pp. 4956–4980, Sep. 2010.
- [8] Y. Shen, H. Wymeersch, and M. Z. Win, “Fundamental limits of wideband localization—part II: Cooperative networks,” *IEEE Trans. Inf. Theory*, vol. 56, no. 10, pp. 4981–5000, Oct. 2010.
- [9] Y. Shen, W. Dai, and M. Z. Win, “Power optimization for network localization,” *IEEE/ACM Trans. on Netw.*, vol. 22, no. 4, pp. 1337–1350, Sep. 2014.
- [10] J. A. Zhang, X. Huang, Y. J. Guo, J. Yuan, and R. W. Heath, “Multibeam for joint communication and radar sensing using steerable analog antenna arrays,” *IEEE Trans. Veh. Technol.*, vol. 68, no. 1, pp. 671–685, Jan. 2019.
- [11] C. B. Barneto, S. D. Liyanaarachchi, T. Riihonen, L. Anttila, and M. Valkama, “Multibeam design for joint communication and sensing in 5G New Radio networks,” in *Proc. IEEE Int. Conf. Comm. (ICC)*, Dublin, Ireland, Jun. 2020.
- [12] Y. Luo, J. A. Zhang, X. Huang, W. Ni, and J. Pan, “Optimization and quantization of multibeam beamforming vector for joint communication and radio sensing,” *IEEE Trans. Commun.*, vol. 67, no. 9, pp. 6468–6482, Sep. 2019.

- [13] H. Asplund, D. Astely, P. von Butovitsch *et al.*, *Advanced Antenna Systems for 5G Network Deployments: Bridging the Gap Between Theory and Practice*. Academic Press, 2020.
- [14] M. A. Richards, *Fundamentals of radar signal processing*. McGraw-Hill, 2005.